Research Article

Mohamed M. Khader* and M. Mohammed Babatin

Numerical investigation of couple stress under slip conditions via modified Adomian decomposition method

https://doi.org/10.1515/phys-2025-0247
Received January 17, 2025; accepted November 14, 2025;
published online December 5, 2025

Abstract: The analysis of couple stress fluids under slip conditions is crucial for optimizing a range of industrial and biomedical applications where microstructural dynamics and interfacial interactions are paramount. Using the slip velocity phenomena, we perform a numerical simulation of magneto-couple stress fluid (CSF) flow over a permeable stretched sheet (SS) inside a porous medium. By employing dimensionless variables, the steady flow model can be converted to a single ordinary differential equation (ODE). Driven by this relevance, our study employs an integrated numerical approach, leveraging the Mohand Transform (MT) and the Adomian Decomposition Method (ADM) to enhance solution precision and ensure robust convergence. The modified ADM simplifies the complex nonlinear equations for efficient computer-based computation, while the Mohand Transform enhances convergence, ensuring that the obtained results closely approach the exact solution. Furthermore, the residual error function is evaluated to verify the accuracy and effectiveness of the developed methodology. When the current findings were compared with other methods for particular flow scenarios, they demonstrated strong agreement, confirming the accuracy of the solution. Research indicates that when coupling stress, suction, and slip velocity parameters are increased, the skin friction coefficient rises; however, when the porous parameter is increased, it falls. The outcomes of this study can be applied to engineering and biomedical systems such as micro-bearings lubrication, small-vessel blood flow, and microfluidic cooling devices.

Keywords: couple stress fluid; slip velocity; MHD; Mohand transforms; modified ADM; residual error function

1 Introduction

The limitations of the Navier–Stokes equations (NSEs) in adequately simulating the flow behavior of non-Newtonian fluids are well known. It is not suitable to utilize the NSEs for the analysis of these fluids because of their complex flow properties, which greatly depart from their basic assumptions. Non-Newtonian fluids have well-known and important applications in many industrial and technological applications. Their special qualities are essential in operations like biomedical engineering, food processing, and polymer synthesis. Because of this, in order to accurately explain and forecast the behavior of these fluids in real-world situations, specialized models and methodologies are frequently needed [1]. The applicability to many industrial applications is apparent when non-Newtonian FF across a stretching sheet is taken into consideration. This situation is especially important for processes like glass blowing [2], where the extrusion of plastic sheets requires a fine surface finish and consistent thickness, and where the controlled stretching of molten glass is necessary for shape [3]. This kind of flow is also relevant to the creation of paper [4], where the material's stretching affects the fibers' alignment and thickness, and to the drawing of copper wires, where stretching allows for exact control over the wire's diameter.

A conducting fluid's properties are usually altered when a magnetic field (MF) is introduced into the flow. Any instabilities in the fluid flow are typically stabilized by this magnetic field. This stabilizing effect may not always hold true, and stability may not always be improved by the magnetic field in the way that is anticipated [5]. Complex behavior can result from the fluid's interaction with the

***Corresponding author: Mohamed M. Khader**, Department of Mathematics and Statistics, College of Science, Imam Mohammad Ibn Saud Islamic University (IMSIU), Riyadh, 11566, Saudi Arabia,
E-mail: mmkhader@imamu.edu.sa
M. Mohammed Babatin, Department of Mathematics and Statistics, College of Science, Imam Mohammad Ibn Saud Islamic University (IMSIU), Riyadh, 11566, Saudi Arabia, E-mail: mmbabatin@imamu.edu.sa

magnetic field; in certain cases, the magnetic field may create new instabilities or change the dynamics of the flow in unexpected ways [6]. The importance of using magnetic fields with electrically conductive fluids in engineering applications is shown in heat generation [7]. In many different metallurgical applications, this approach is especially significant. Engineers are able to control this cooling process accurately, which affects the characteristics and quality of the metals that are created. This is achieved by introducing a magnetic field. Greater control over the structural and mechanical properties of the material is made possible by this magnetic manipulation, and this control is essential for obtaining the intended results in manufacturing and industrial operations [8]. Recent research underscores the significance of magnetic fields, slip velocity, and the mechanism of fluid flow in optimizing heat transfer and flow control over deformable surfaces. Studies by Rashid et al. [9–11], and Atif et al. [12] collectively demonstrate how these phenomena govern thermal and hydrodynamic performance. Building on these findings, this work systematically investigates their coupled effects in fluid flow systems, advancing predictive models for engineering applications.

As an expansion of the conventional viscous theory, Stokes [13] created the notion of the CSF. With the inclusion of a couple stress & body couples, this new theory offers a more thorough framework for the analysis of fluid mechanics. The theory makes it possible to analyze complex fluid behaviors that are not well explained by conventional viscosity theory by including these extra forces. This advancement has expanded the field of fluid dynamics and made it possible to represent fluid interactions and phenomena in the actual world with greater accuracy. The couple stress fluid model accurately characterizes fluids exhibiting microstructural interactions and intrinsic rotational effects beyond Newtonian approximations, making it ideal for systems with suspended particulates or microscale flow geometries. This framework proves valuable for analyzing blood flow, specialized lubricants, and electro-rheological fluids, as well as industrial processes like precision coating and polymer extrusion. Its capability to resolve micro-rotational dynamics also enhances the modeling of biological flows (e.g., synovial fluid or capillary blood circulation) and engineered systems involving porous media or magnetic fields, justifying its use in this study of complex non-Newtonian transport phenomena [14]. Given the critical relevance of this type of fluid, numerous researchers [15–18] have investigated their behavior across diverse physical conditions and industrial contexts. These studies demonstrate their efficacy in optimizing thermal and hydrodynamic performance in engineered systems.

The model in question simplifies to a highly nonlinear ODE, for which an exact analytical solution is sometimes impossible. Therefore, to get an approximate or numerical solution, one must use one of the well-known and highly accurate numerical techniques. A number of sophisticated numerical and semi-analytical approaches are available for tackling complex fluid flow models of substantial physical importance. Prominent among these are the Adomian Decomposition Method [19], the Finite Volume Method [20], and the Homotopy Analysis Method [21]. The selection of these methods is often justified by their documented reliability, accuracy, and adaptability in resolving the nonlinear systems inherent to fluid dynamics and thermal processes. The extensive body of literature utilizing these techniques attests to their robust potential for modeling fundamental physical behavior and generating stable, convergent outcomes in a multitude of applied scenarios.

We addressed the problem analytically using a newly developed methodology. This strategy utilized a modified ADM model combined with MT [22]. This new approach offers greater accuracy and efficiency, making it a good method for solving difficult analytical problems. This method sometimes provides the exact solutions to the problem under study. The solution to the emerging of the ODE verifies the validity and usefulness of this approach. Graphs and tables are employed to simulate the collected data.

This research aims to do an extensive analysis of the behavior of the CSF flows over the SS, especially when a magnetic field is present and the fluid passes through a porous medium. The purpose of the current work is to comprehend the intricate dynamics and interactions that take place in these situations. The research aims to provide important insights into the influences of pair stresses, magnetic fields, and porous media on fluid flow by investigating this scenario. These findings may have important ramifications for many industrial applications. An effective method for solving the model equations is the ADM. The MT is applied in addition to this approach. These two methods are combined in the study to effectively address the model's intricacies and enable a more accurate and effective solution. Through a deep look into the behavior of the system under investigation, this hybrid approach improves analytical capacities [23,24]. In article [25], the authors presented a new analytical technique (ADM with MT) and applied it to obtain analytical solutions to a system of PDEs in their fractional form (Cabuto). In [26], the authors introduced the approximate solution of the Kersten-Krasil'shchik coupled KdV by employing the natural transform and the ADM. In

[27], the Laplace-ADM is implemented to solve the fractional telegraph equations.

While the phenomena of couple stress and slip flow have been widely examined, the combined impact of suction, slip velocity, and a porous medium on magneto-couple stress fluids remains a relatively unexplored area. Existing research, often limited to purely analytical or numerical approaches, can struggle with convergence and accurately modeling the complete physics of these complex systems. To bridge this gap, the current work presents a novel hybrid technique that integrates the MT with the ADM. This synergy yields robust semi-analytical solutions that effectively circumvent previous limitations. The primary novelty of this research is the successful application of this integrated solver to precisely model couple stress fluid flow under realistic boundary conditions. Consequently, its key contribution is the delivery of new physical insights into the interdependent roles of slip, suction, and porous parameters on flow and thermal fields, with significant implications for advanced engineering and biomedical design.

1.1 Main contributions and novel insights

This study introduces a new examination of magneto-couple stress fluid flow over a permeable SS in a porous medium, notably including slip velocity, a less-explored area. The primary contribution is a novel hybrid analytical-numerical technique, combining the Mohand transform with the ADM, which ensures quick convergence and higher solution accuracy. This method simplifies complex nonlinear equations and its results align well with established benchmarks. Furthermore, the research offers fresh insights into how key parameters like couple stress, suction, slip velocity, and porosity affect the skin friction coefficient, thereby enhancing our understanding of slip flow behavior in magneto-porous systems.

The construction of the manuscript is presented in the following order: Section 2 introduces the mathematical development of the model under study. Section 3 delineates the procedure solution, where we presented some essential ideas on the MT and implemented modified ADM. Section 4 gives a code verification for the proposed method. Section 5 shows a numerical simulation of the examination problem and a discussion of the results obtained. Section 6 presents the conclusions.

2 Mathematical development

Considering the steady-state, fluid flow of a non-Newtonian CSF across a linearly permeable SS during a porous medium. Perpendicular to the permeable, stretchy surface, a specific strength of the MF is applied. The fluid movement in the surrounding area may be affected by this field's interaction with the flow dynamics because of the magnetohydrodynamic (MHD) effects. The flow happens in the semi-infinite porous zone where $y > 0$, which is described by its permeability, and the permeable sheet is deemed to line with $y = 0$ (see Figure 1). As it is clear, Figure 1 schematically depicts the studied configuration: a 2D magneto-couple stress fluid flowing steadily over a porous, SS aligned with the $x-$ axis. The model incorporates transverse magnetic effects ($y-$ direction), and wall-normal flow development, and accounts for both surface suction/injection and velocity slip boundary conditions.

The stretching velocity of the sheet is given by $u_w = bx$; b is the stretching rate. This suggests that the sheet extends faster the farther you walk along it and that the pace of stretching is directly related to the distance x from a given location. The objective is to compute the fluid's velocity field, especially in the involvement of the slip velocity phenomenon at the permeable SS and at locations remote from it that satisfy the necessary boundary constraints. The momentum and continuity equations for the couple stress fluid are systematically derived, incorporating the steady, incompressible flow conditions, boundary layer approximations, Darcy-porous medium interactions, and transverse magnetic field effects. The mathematical formulation rigorously accounts for microstructural stresses characteristic of non-Newtonian fluids, while ensuring consistency with fundamental conservation laws [28]:

$$\nabla \cdot U = 0, \tag{1}$$

$$U \cdot \nabla U = \frac{\mu}{\rho}(\nabla \times \nabla \times U) - \frac{\eta_0}{\rho}(\nabla \times \nabla \times \nabla \times \nabla \times U) - \frac{\mu}{\rho k}U - \frac{\sigma B_0^2}{\rho}U, \tag{2}$$

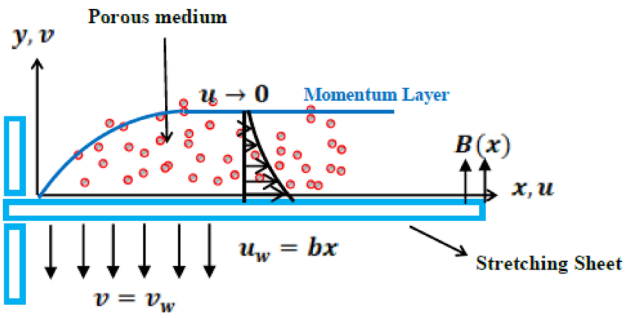

Figure 1: Geometrical model and coordinate system of the FF.

where $U = (u, v)$, ρ, k, μ, σ, and B_0, are the velocity vector, density, permeability, viscosity, electrical conductivity, and the magnetic field intensity, respectively. Now, we simplify the continuity and momentum equations by using the boundary layer approximation. In this approximation, the area near the sheet where the fluid undergoes abrupt velocity changes is the main focus. As a result, we arrived at the subsequent governing equations [29]:

$$u_x + v_y = 0, \tag{3}$$

$$u\,u_x + v\,u_y + \frac{\eta_0}{\rho}u_{yyyy} = \frac{\mu}{\rho}u_{yy} - \frac{\mu}{\rho\,k}u - \frac{\sigma B_0^2}{\rho}u, \tag{4}$$

here, η_0 denotes the material constant specific to the couple stress fluid, which characterizes its unique properties. Here, it is important to see that the non-Newtonian CSF can be made into a Newtonian fluid by setting the material couple stress parameter to zero ($\eta_0 = 0$). This will remove the couple stresses' effects and simplify the fluid's behavior to that of a typical Newtonian fluid. The CSF is the electric conductivity. The following boundary conditions (B.Cs), which must be satisfied to characterize the CSF's behavior inside the system, control its flow:

$$\begin{aligned} u = u_w &= bx + \beta_0\left[\left(\frac{\partial u}{\partial y}\right) - \frac{\eta_0}{\mu\rho}\left(\frac{\partial^3 u}{\partial y^3}\right)\right], \\ v = -v_w, &\qquad \frac{\partial^2 u}{\partial y^2} = 0, \quad \text{at} \quad y = 0, \end{aligned} \tag{5}$$

$$u \to 0, \qquad \frac{\partial u}{\partial y} \to 0, \qquad \text{at} \qquad y \to \infty. \tag{6}$$

The velocity slip coefficient β_0 controls the preceding boundary conditions. It takes into consideration the relative motion of the fluid and the boundary surface, permitting partial slip instead of a no-slip condition. Incorporating slip velocity is essential for modeling realistic flow behavior in microscale and nanoscale systems where the no-slip condition breaks down due to surface interactions, roughness, or rarefaction effects. Slip alters velocity profiles, reduces shear stress, and modifies near-wall heat and mass transfer – critical for micro/nanofluidic devices, MEMS lubrication, polymer processing, and targeted drug delivery. This approach enhances accuracy in predicting flow dynamics for such applications.

2.1 Model in dimensionless form

Here, by lowering the number of independent parameters, the problem can be made simpler by applying similarity transformations. Thus, with the help of similarity transformations, the controlling nonlinear PDEs are converted to dimensionless ODE, which can be described as follows [30]:

$$\begin{aligned} \eta = \left(\frac{b\rho}{\mu}\right)^{\frac{1}{2}} y, \qquad u = bx f'(\eta), \\ v = -\left(\frac{b\mu}{\rho}\right)^{\frac{1}{2}} f(\eta). \end{aligned} \tag{7}$$

In the context of our investigation, this equation, which directly results from the transformations, is crucial for additional analysis:

$$K f^{(5)} - f''' - f f'' + f'^2 + (\lambda + M) f' = 0, \tag{8}$$

$$\begin{aligned} f(\eta) = \omega, \qquad f'(\eta) = 1 + \beta\left(f'' - K f^{(4)}\right), \\ f'''(\eta) = 0, \qquad \text{at} \quad \eta = 0, \end{aligned} \tag{9}$$

$$f'(\eta) \to 0, \qquad f''(\eta) \to 0, \qquad \text{as} \quad \eta \to \infty. \tag{10}$$

Here $\lambda = \frac{\mu}{bk\rho}$ is the porous parameter, $M = \frac{\sigma}{\rho b}B_0^2$ is the MF parameter, $K = \frac{\eta_0 b}{\nu^2 \rho}$ is the couple stress parameter, $\omega = \frac{-v_w}{\sqrt{\nu b}}$ is the suction parameter and $\beta = \beta_0\sqrt{\frac{b}{\nu}}$ is the slip velocity parameter. We will now continue the study by discussing the skin friction coefficient (SFC) Cf_x, an important parameter of fluid dynamics. It measures the resistance that a fluid encounters when it comes into contact with a solid surface, and its comprehension is crucial for maximizing flow rates, reducing energy waste, and guaranteeing the effectiveness of a range of technical applications. The following represents a representation of the skin friction coefficient formula:

$$Cf_x = \frac{\tau_w}{\rho u_w^2}, \tag{11}$$

where τ_w takes the following form:

$$\tau_w = -\left[\mu\left(\frac{\partial u}{\partial y}\right) - \frac{\eta_0}{\rho}\left(\frac{\partial^3 u}{\partial y^3}\right)\right]_{y=0}. \tag{12}$$

Using equation (12) and the non-dimensional variables provided in equation (7) in conjunction with the relationship described in equation (11), we arrive at the following conclusion:

$$Cf_x \mathrm{Re}^{\frac{1}{2}} = -\left[f''(0) - K f^{(4)}(0)\right], \tag{13}$$

where $\mathrm{Re} = \frac{u_w x}{\nu}$ is the local Reynolds number.

3 Procedure solution

3.1 Basic concepts on the MT

The MT of the function $g(\eta)$ is denoted and given as follows [31]:

$$\mathbb{M}\{g(\eta)\} = G(\varrho) = \varrho^2 \int_0^\infty g(\eta) \mathrm{e}^{-\varrho\,\eta} \mathrm{d}\eta, \qquad k_1 \le \varrho \le k_2.$$

The inverse MT of $G(\varrho)$ is $\mathbb{M}^{-1}\{G(\varrho)\} = g(\eta)$.

The main properties of the MT [32]:

1. For arbitrary constants a_1, a_2, we have

$$\mathbb{M}\{a_1 g_1(\eta) + a_2 g_2(\eta)\} = a_1 \mathbb{M}\{g_1(\eta)\} + a_2 \mathbb{M}\{g_2(\eta)\}.$$

2. The MT of the derivatives $g^{(n)}(\eta)$.

$$\mathbb{M}\left\{g^{(n)}(\eta)\right\} = \varrho^n G(\varrho) - \varrho^{n+1} g(0) - \varrho^n g'(0) - \cdots - \varrho^2 g^{(n-1)}(0), \qquad n = 1, 2, \ldots. \tag{14}$$

3. The MT for the power functions:

$$\mathbb{M}\{\eta^n\} = \begin{cases} \dfrac{n!}{\varrho^{n-1}}, & n \in \mathbb{N}; \\ \dfrac{\Gamma(n+1)}{\varrho^{n-1}}, & n > -1. \end{cases}$$

3.2 Implementation of the modified ADM

To apply the modified ADM for solving equation (8), we reform it in the following form:

$$f^{(5)}(\eta) = \mathrm{NL}(f) = K^{-1}\left[f''' + f\,f'' - f'^2 - (\lambda + M) f'\right]. \tag{15}$$

Taking the MT of this model (15) gives the following:

$$s^5 F(s) - s^6 f(0) - s^5 f'(0) - s^4 f''(0) - s^3 f'''(0) - s^2 f^{(4)}(0) = \mathbb{M}\left[\mathrm{NL}(f)\right]. \tag{16}$$

By imposing the B.Cs (9), we can get the following solution:

$$F(s) = s\,\omega + \chi_1 + \frac{1}{s}\chi_2 + \frac{1}{s^3}\chi_3 + \frac{1}{s^5}\mathbb{M}\left[\mathrm{NL}(f)\right]. \tag{17}$$

Taking the inverse MT of the equation (17) yields the following:

$$f(\eta) = \omega + \chi_1 \eta + \frac{1}{2}\chi_2 \eta^2 + \frac{1}{24}\chi_3 \eta^4 + \mathbb{M}^{-1}\left[\frac{1}{s^5}\mathbb{M}\left[\mathrm{NL}(f)\right]\right], \tag{18}$$

where

$$\chi_1 = f'(0), \qquad \chi_2 = f''(0), \qquad \chi_3 = f^{(4)}(0).$$

Now, the components of the approximate solution to the problem under study will be obtained using the iterative scheme as follows:

$$\bar{f}_0(\eta) = \omega + \chi_1 \eta + \frac{1}{2}\chi_2 \eta^2 + \frac{1}{24}\chi_3 \eta^4, \tag{19}$$

$$\bar{f}_{m+1}(\eta) = \mathbb{M}^{-1}\left[\frac{1}{s^5}\mathbb{M}\left[\mathrm{NL}(f)\right]\right] = \mathbb{M}^{-1}\left[\frac{1}{s^5}\mathbb{M}\left[A_m\right]\right], \qquad m = 1, 2, \ldots. \tag{20}$$

We decompose the nonlinear term $\mathrm{NL}(f)$ by utilizing Adomian's polynomials A_m in the following form:

$$\mathrm{NL}(f) = \sum_{m=0}^{\infty} A_m, \tag{21}$$

where,

$$A_m = \frac{1}{m!}\left[\frac{\mathrm{d}^m}{\mathrm{d}\lambda^m}\left[\mathrm{NL}\left(\sum_{i=0}^{\infty}\theta^i \bar{f}_i\right)\right]\right]_{\theta=0}. \tag{22}$$

Applying the previous formula, we can calculate the first A_m in the following form:

$$\begin{aligned} A_0 &= K^{-1}\left[\bar{f}_0''' + \bar{f}_0\bar{f}_0'' - \bar{f}_0'^2 - (\lambda + M)\bar{f}_0'\right] \\ &= K^{-1}\left[\left(\omega + \chi_1\eta + \frac{1}{2}\chi_2\eta^2 + \frac{1}{24}\chi_3\eta^4\right)\chi_2 - \chi_1^2 - (\lambda + M)\chi_1\right], \\ A_1 &= K^{-1}\left[\bar{f}_1''' + \bar{f}_0\bar{f}_1'' + \bar{f}_1\bar{f}_0'' - 2\bar{f}_0'\bar{f}_1' - (\lambda + M)\bar{f}_1'\right], \ldots. \end{aligned} \tag{23}$$

We can calculate the first components of the approximate solution using the iterative formula (20) in the following form:

$$\begin{aligned} \bar{f}_1(\eta) &= \mathbb{M}^{-1}\left[\frac{1}{s^5}\mathbb{M}\left[A_0\right]\right] \\ &= K^{-1}\left[\left(\frac{1}{5!}\omega\eta^5 + \frac{1}{6!}\chi_1\eta^6 + \frac{1}{7!}\chi_2\eta^7 + \frac{1}{9!}\chi_3\eta^9\right) \times \chi_2 - \frac{1}{5!}\eta^5\left(\chi_1^2 + (\lambda + M)\chi_1\right)\right], \ldots. \end{aligned} \tag{24}$$

Thus, we can obtain the approximate solution by collecting m of these approximated terms as follows:

$$f_m(\eta) = \sum_{k=0}^{m-1} \bar{f}_k(\eta). \tag{25}$$

When $m \to \infty$, this form is close to the true solution.

The values of $\chi_k, k = 1, 2, 3$ will be given by applying the B.Cs (9)-(10).

To achieve a complete numerical simulation, we estimate the following residual error function $\mathrm{REF}_f(m, \eta)$ [33] for the solution $f(\eta)$ of equation (8) as follows:

$$\mathrm{REF}_f(m,\eta) = K\, f_m^{(5)}(\eta) - f_m^{(3)}(\eta) - f_m(\eta) f_m^{(2)}(\eta) + (f_m'(\eta))^2 + (\lambda + M)\, f_m'(\eta) \simeq 0. \quad (26)$$

The convergence of the ADM is well known and has been discussed and studied in many studies, including [34–36]. Here, in this paper, the method has been improved by applying the Mohand transform. Therefore, the accuracy of the modified method will be verified in the next section, as is the case in many recently published studies, such as [37,38]. This is done through comparisons with other methods, as well as calculating the REF, and also through graphical results, which demonstrate the high agreement between the approximate solutions and the solution behavior, while achieving the expected physical meanings for the problem under study.

4 Code verification

The modified ADM was used to numerically solve the nonlinear ODE (8) and the associated B.Cs. Figures are used to show the significance of the physical parameters. Data from the literature, according to Turkyilmazoglu [39], and Yih [40] (who used the finite difference method) have been compared in Table 1 with our findings for the SF-coefficient $-f''(0)$.

To validate our approximate solutions at ($K = 0.5, \beta = M = 0.3, \lambda = 0.2, \omega = 0.8$), we give a comparison in Table 2 with the ADM [41, 42] with different values of m by computing the REF in the two methods. This comparison illustrates the thoroughness of the introduced method in this paper. From the REF, we can confirm that the accuracy of the method can be controlled by choosing appropriate values for the approximation order m.

Table 1: Values of $-f''(0)$ at various λ with $K = \beta = \omega = M = 0$.

λ	Turkyilmazoglu [39]	Yih [40]	Present work
0.0	1.00000000	1.0000000000	1.0000000000
0.5	1.22474487	1.2247000000	1.2247447998
1.0	1.41421356	1.4142000000	1.4142135550
1.5	1.58113883	1.5811000000	1.5811388259
2.0	1.73205081	1.7321000000	1.7320507995

Table 2: A comparison of the REF between the current method and the ADM via various values of m.

η	Present Method–REF at:		ADM–REF at:	
	$m = 7$	$m = 13$	$m = 7$	$m = 13$
0.0	6.75364E−06	9.12550E−10	3.25478E−04	6.02517E−07
0.6	1.74102E−06	4.14785E−09	6.02584E−03	7.25810E−06
1.2	2.95142E−05	7.52841E−09	5.21470E−03	5.22581E−06
1.8	3.02541E−06	6.25874E−09	0.65471E−03	4.25910E−05
2.4	5.00442E−05	6.02584E−08	9.02547E−02	5.01487E−04
3.0	1.25874E−04	6.25874E−07	0.21450E−02	7.25644E−04

5 Results and discussion

By combining the modified ADM for solving the nonlinear ordinary differential equation and related boundary conditions is created. By combining these two approaches, the analytical process is streamlined, and the complexity of nonlinear systems may be effectively handled. It produces solutions that are more accurate and efficient, and provides significant insights into the behavior of the model. It is especially helpful in solving nonlinear differential equations when dealing with boundary conditions, which makes it an invaluable tool in both mathematics and engineering contexts. We shall provide a detailed analysis of the non-Newtonian CSF flow across the SS embedded in a porous medium in this section. Keeping all other factors fixed, Figure 2 looks at how changes in both K and β affect $f(\eta)$ and $f'(\eta)$. It can be seen that for $0.0 < \eta < 3.0$, the velocity increases as both K and β increase. By altering the shear stress distribution, K, in the meantime, takes into consideration the stresses and micro-rotational effects inside the fluid, which can improve the fluid's flow characteristics. When combined, these factors lower the total flow resistance and encourage a faster flow rate within the designated range of η. Furthermore, the couple stress parameter causes the dimensionless stream function to grow, whereas the slip velocity parameter causes the opposite effect. Physically, the couple stress parameter characterizes the microscale rotational behavior within the fluid, leading to the development of asymmetric stresses that decrease viscous resistance and enhance the overall flow velocity. At the same time, the presence of velocity slip minimizes wall shear by reducing fluid–surface interaction, thereby facilitating faster motion near the boundary. Together, these two effects – microstructural rotation and interfacial slip act synergistically to improve momentum transfer and alter the structure of the boundary layer.

Variations in λ and M are shown to affect the $f(\eta)$ and $f'(\eta)$ profiles in Figure 3. About the overall fluid dynamics, the effects of these parameters are highlighted, and insights into the flow behavior under various porosity and magnetic influence circumstances are provided by this graphical representation. Reduced fluid velocity and a dimensionless stream function result from the magnetic field's

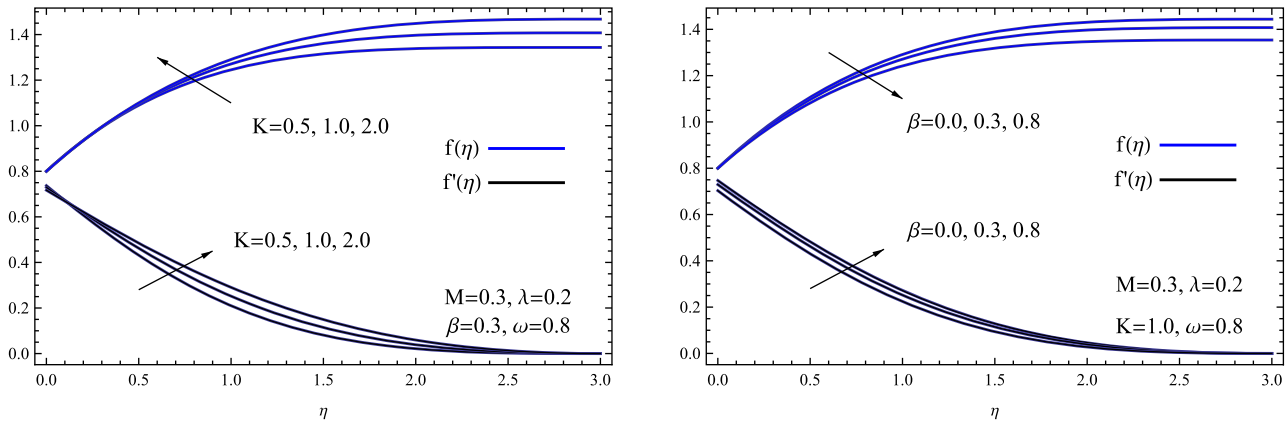

(a) $f(\eta)$ and $f'(\eta)$ for selected K (b) $f(\eta)$ and $f'(\eta)$ for selected β

Figure 2: The influence of K and β on $f(\eta)$ and $f'(\eta)$. (a) $f(\eta)$ and $f'(\eta)$ for selected K (b) $f(\eta)$ and $f'(\eta)$ for selected β.

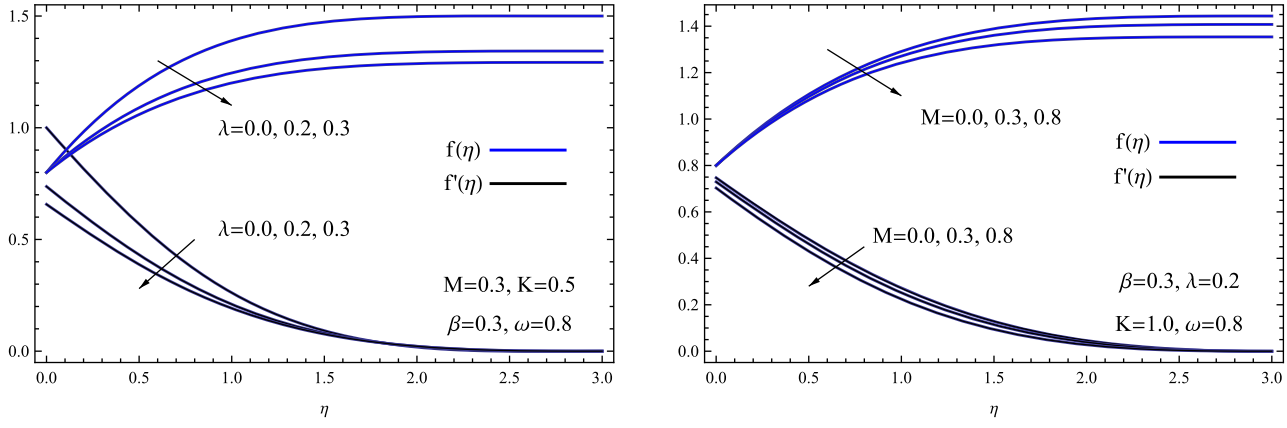

(a) $f(\eta)$ and $f'(\eta)$ for selected λ (b) $f(\eta)$ and $f'(\eta)$ for selected M

Figure 3: The influence of λ and M on $f(\eta)$ and $f'(\eta)$. (a) $f(\eta)$ and $f'(\eta)$ for selected λ (b) $f(\eta)$ and $f'(\eta)$ for selected M.

opposition to the fluid's motion, or Lorentz force. Due to the introduction of resistance to the flow through the medium, the porous parameter exhibits the same behavior. In a manner akin to the Lorentz force, the porous structure reduces the fluid's velocity and modifies the stream function by raising friction and decreasing total permeability. From a physical perspective, both the applied magnetic field and the porous medium act as resistive forces that impede fluid motion. The magnetic field induces a Lorentz force opposing the fluid's movement, thereby diminishing its velocity and stream function. Concurrently, the limited permeability of the porous medium enhances viscous drag, which further suppresses fluid motion and weakens circulation intensity. The combined influence of these resistive mechanisms markedly affects momentum transport within magneto-porous configurations. Such behavior is critical in the MHD flow control applications, including nuclear reactor cooling, microfluidic systems, and biomedical processes, where accurate magnetic regulation of fluid dynamics is essential.

Figure 4 compares two cases: One without a porous medium ($\lambda = 0.0$) and another with a porous medium present ($\lambda = 0.3$). In the absence of porosity ($\lambda = 0.0$), the streamlines follow a smooth, uninterrupted path, indicating undisturbed flow. However, when porosity is introduced ($\lambda = 0.3$), the streamlines become scattered, revealing how the porous structure disrupts the flow by redirecting pathways and adding complexity. This contrast indicates the significant impact of porous media on fluid dynamics. From a physical standpoint, introducing a porous medium enhances resistance to fluid motion, forcing the fluid particles to diverge from their normal trajectories. As a result, the

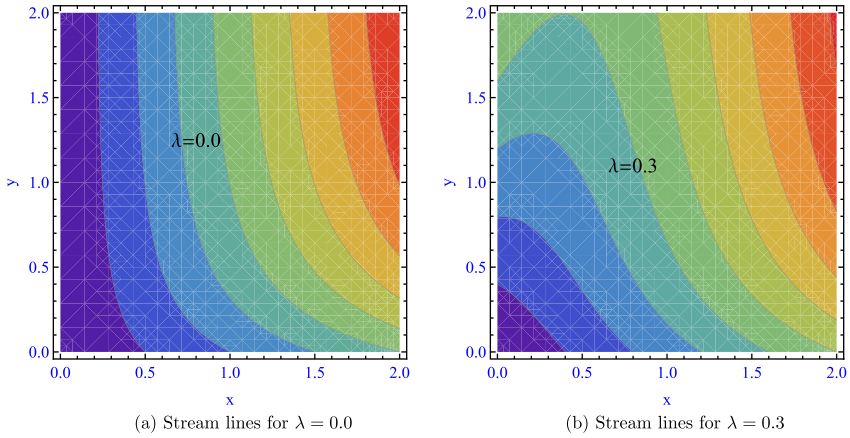

Figure 4: Stream lines for different λ. (a) For λ=0.0 (b) For λ=0.3.

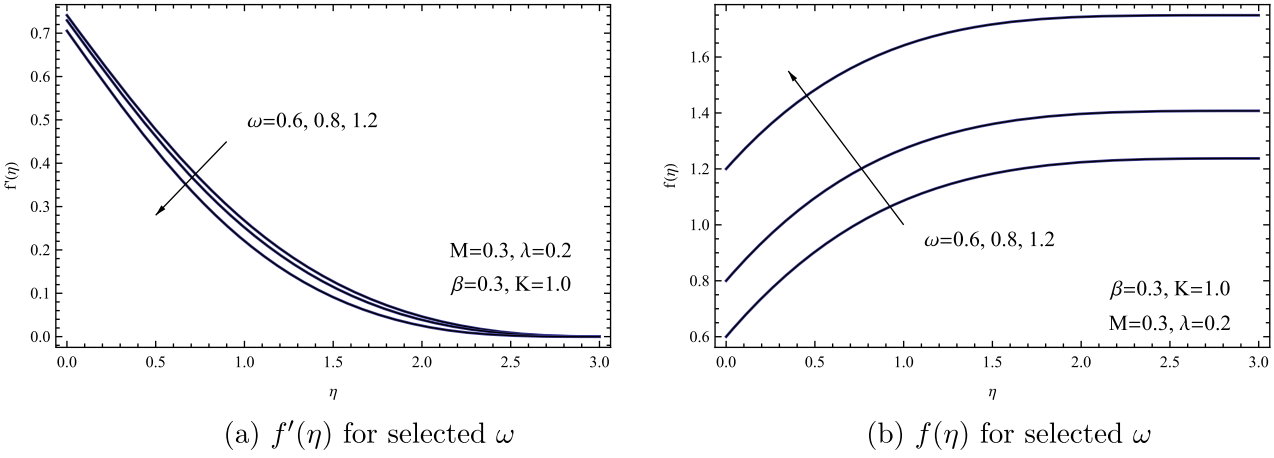

Figure 5: The influence of ω on $f(\eta)$ and $f'(\eta)$. (a) $f'(\eta)$ for selected ω (b) $f(\eta)$ for selected ω.

streamlines become irregular and disturbed, demonstrating the dissipative and energy-attenuating influence exerted by the porous matrix.

The relationship between $f(\eta)$ and $f'(\eta)$ is clarified in Figure 5 by the suction parameter ω. A thorough illustration of how different suction levels affect the flow characteristics is given by this visualization. The fluid velocity falls and the dimensionless stream function rises as the suction parameter varies. Higher suction causes fluid to be removed from the BL, which raises the concentration of fluid close to the surface and intensifies the velocity gradient. As a result, the dimensionless stream function rises as it represents the improved flow dynamics close to the boundary, but the overall fluid velocity falls as a result of the fluid removal. Physically, a higher suction parameter pulls fluid away from the surface, which intensifies the velocity gradient close to the boundary and increases the stream function. Nevertheless, this removal of fluid leads to a decrease in the overall fluid velocity, as less fluid remains within the boundary layer.

Finally, through all these discussions and physical interpretations of all the parameters affecting the problem under study, which indicate that the expected physical meanings of the solution's behavior are achieved, this means that the proposed method has been applied well, more effectively, and accurately.

Table 3 gives the relationship between the SFC and the other governing parameters, such as the suction, slip velocity, porous, magnetic, and couple stress characteristics. This table gives a thorough summary of how each of these variables affects the skin friction coefficient, a crucial component in figuring out the resistance a fluid encounters when it passes over a surface. By looking at these variances, the table helps clarify how these parameters interact and how they affect skin friction as a whole, providing important insights into how the fluid behaves generally in response to changes in these controlling elements. This table shows that while λ shows the opposite trend, K, β, M, and ω all show a rise in skin friction coefficient with rising values. This

Table 3: Skin friction coefficient $Cf_x \mathrm{Re}^{\frac{1}{2}}$ as a function of specific controlling parameters.

K	β	λ	M	ω	$Cf_x \mathrm{Re}^{\frac{1}{2}}$
0.5	0.3	0.2	0.3	0.8	1.31513
1.0	0.3	0.2	0.3	0.8	1.35283
2.0	0.3	0.2	0.3	0.8	1.41494
1.0	0.0	0.2	0.3	0.8	1.26480
1.0	0.3	0.2	0.3	0.8	1.35283
1.0	0.8	0.2	0.3	0.8	1.48473
0.5	0.3	0.0	0.3	0.8	1.93024
0.5	0.3	0.2	0.3	0.8	1.31513
0.5	0.3	0.3	0.3	0.8	1.14272
1.0	0.3	0.2	0.0	0.8	1.26481
1.0	0.3	0.2	0.3	0.8	1.35283
1.0	0.3	0.2	0.8	0.8	1.48473
1.0	0.3	0.2	0.3	0.6	1.29326
1.0	0.3	0.2	0.3	0.8	1.35283
1.0	0.3	0.2	0.3	1.2	1.47325

result indicates that elements that either improve the fluid-surface interaction or increase the flow resistance have a direct impact on skin friction. More specifically, because of increased fluid resistance and surface interactions, higher skin friction is caused by increases in K, β, M, and ω. On the other hand, a larger porosity parameter lowers skin friction by making it easier for fluid to move through the porous medium, which lowers resistance and surface interaction. Finally, this study provides actionable insights with direct implications for engineering and biomedicine. The elucidated relationships between key parameters, slip, suction, and porosity and the resulting flow offer a blueprint for optimizing thermal management systems. Such optimization is vital in contexts ranging from nuclear power generation to electronics cooling. Additionally, the results provide critical guidance for the design of next-generation microfluidic devices, where precise control over minute fluid volumes is paramount for biomedical diagnostics.

6 Conclusions

This research presented a novel computational framework that leverages the MT and ADM to analyze the steady flow of a non-Newtonian couple stress fluid over a stretching sheet embedded in a Darcy porous medium, under the influence of slip velocity and magnetic fields. The present work discloses the intricate interplay between fluid microstructure, boundary slip, and magnetic forces, transforming the resulting equations into a dimensionless form for analytical solutions. Graphically illustrated velocity and stream function profiles reveal their sensitivity to various physical parameters. Key contributions include a modified semi-analytical technique with improved convergence, a detailed parametric investigation of flow responses to magnetic intensity, suction, slip, and couple stress effects, and rigorous validation against existing studies. In summary, the findings have demonstrated that:

1. A thinner boundary layer is produced when the velocity distribution is retarded by a boost in the suction, porosity, and magnetic parameters.
2. The slip and coupling stress parameters also rise in tandem with the velocity profiles.
3. Significant effects on the Cf_x can be observed as the slip, magnetic, porous, and couple stress parameters grow.
4. Flow through a porous medium shows an inverse relationship with the coefficient of skin friction, resulting in a significant decrease in it.
5. Raising the quantities of K and ω results in a higher dimensionless stream function.
6. Future research could expand this model to better reflect real-world conditions by incorporating 3D flow dynamics, temperature-sensitive material properties, and machine learning algorithms. These enhancements would improve both the precision and computational performance of the solutions.

In addition, by comparing our results with other methods and calculating the residual error function, as well as verifying the expected physical meanings of the solution behavior, this means that the given method has been well implemented and is more effective and accurate. In future work, we will try to study convergence by presenting a theoretical study to prove it, as well as making further modifications to the proposed method to avoid shortcomings and to increase the accuracy of the solutions and the efficiency of the technique. Also, we try to solve this problem using other methods, such as the finite element method or finite difference method.

Acknowledgments: This work was supported and funded by the Deanship of Scientific Research at Imam Mohammad Ibn Saud Islamic University (IMSIU) (grant number IMSIU-DDRSP2503).
Funding information: This work was supported and funded by the Deanship of Scientific Research at Imam Mohammad Ibn Saud Islamic University (IMSIU) (grant number IMSIU-DDRSP2503).
Author contribution: All authors have accepted responsibility for the entire content of this manuscript and approved its submission.
Conflict of interest: The authors state no conflict of interest.

Data availability statement: All data generated or analysed during this study are included in this published article.

References

1. Megahed AM. Variable viscosity and slip velocity effects on the flow and heat transfer of a power-law fluid over a non-linearly stretching surface with heat flux and thermal radiation. Rheol Acta 2012;51:841—74.
2. Liu IC, Megahed AM, Hung HW. Heat transfer in a liquid film due to an unsteady stretching surface with variable heat flux. ASME J Appl Mech 2013;80:041003.
3. Megahed AM, Gnaneswara R, Abbas W. Modeling of MHD fluid flow over an unsteady stretching sheet with thermal radiation, variable fluid properties, and heat flux. Math Comput Simulat 2021;185:583—93.
4. Amer AM, Ghoneim IN, Megahed AM. Investigation of dissipation phenomenon of non-Newtonian nanofluid due to a horizontal stretching rough sheet through a Darcy porous medium. Appl Eng Sci 2024;17:100171.
5. Ali N, Khan SU, Abbas Z. Hydromagnetic flow and heat transfer of a Jeffrey fluid over an oscillatory stretching surface. Z Naturforsch 2015;70:567—76.
6. Turkyilmazoglu M. An analytical treatment for the exact solutions of MHD flow and heat over three-dimensional deforming bodies. Int J Heat Mass Tran 2015;90:781—9.
7. Naz R, Tariq S, Sohail M, Shah Z. Investigation of entropy generation in stratified MHD Carreau nanofluid with gyrotactic microorganisms under Von Neumann similarity transformations. Eur Phys J Plus 2020;135:178.
8. Dadheech A, Parmar A, Agrawal K, Al-Mdallal Q, Sharma S. Second law analysis for MHD slip flow for Williamson fluid over a vertical plate with Cattaneo-Christov heat flux. Case Study Therm Eng 2022;33:101931.
9. Rashid U, Baleanu D, Liang H, Abbas M, Iqbal A, Rahman J. Marangoni boundary layer flow and heat transfer of Graphene-Water nanofluid with particle shape effects. Processes 2020;8:1—17.
10. Rashid U, Baleanu D, Iqbal A, Abbas M. Shape effect of nanosize particles on magnetohydrodynamic nanofluid flow and heat transfer over a stretching sheet with entropy generation. Entropy 2020;22:1—12.
11. Rashid U, Liang H, Ahmad H, Abbas M, Iqbal A, Hamed YS. Study of (Ag and TiO_2) water nanoparticles shape effect on heat transfer and hybrid nanofluid flow toward stretching shrinking horizontal cylinder. Results Phys 2021;21:1—8.
12. Atif SM, Abbas M, Rashid U, Emadifar H. Stagnation point flow of EMHD micropolar nanofluid with mixed convection and slip boundary. Complexity 2021;3754922:1—13.
13. Stokes VK. Couple stress in fluids. Phys Fluids 1966;9:1709—15.
14. Srinivasacharya D, Kaladhar K. Soret and Dufour effects in a mixed convection couple stress fluid with heat and mass fluxes. Lat Am Appl Res 2011;41:353—8.
15. Ramzan M. Influence of Newtonian heating on three-dimensional MHD flow of couple stress nanofluid with viscous dissipation and Joule heating. PLoS One 2015;10:10e0124699.
16. Sithole H, Mondal H, Goqo S, Sibanda P, Motsa S. Numerical simulation of couple stress nanofluid flow in magneto-porous medium with thermal radiation and a chemical reaction. Appl Math Comput 2018;339:820—36.
17. Abu-Shaikha MF, Abbas Z, Rafiq MY, Fayyaz A. Influence of motility on couple stress fluid flow through a channel with slip constraints. Case Stud Therm Eng 2025;72:106234.
18. Alrihieli H, Aldhabani MS. Analysis of dissipative slip flow in couple stress nanofluids over a permeable stretching surface for heat and mass transfer optimization. Case Stud Therm Eng 2025;67:105819.
19. Tich MST, Kezzar M, Usman ASA, Khalifa HAE, Znaidia S, Sari MR. Ohmic dissipation on Jeffery-Hamel flow of an electrically conducting second-grade fluid in converging and diverging channels under velocity slip effects: semi-analytical simulations via ADM. Adv Theor Simul 2025;8:1—11.
20. Kehil MS, Nacereddine MK, Usman BF, Filali A, Darvesh A, Kezzar M, et al. MHD natural convection in a differentially heated cavity filled with a Cu-water nanofluid using FVM. Case Stud Therm Eng 2025;72:1—14.
21. Shamshuddin MD, Shah Z, Usman SN, Alshehri MH, Vrinceanu N, Antonescu E, et al. Investigation of convective heat transport in a Carreau hybrid nanofluid between two stretchable rotatory disks. Open Phys 2024;22:1—14.
22. Sudhanshu A, Rashmi M, Anuj K. A comparative study of Mohand and Elzaki transforms. Glob J Eng Sci Res 2019;6:203—13.
23. Mohand M, Mahgoub A. The new integral transform Mohand transform. Adv Theor Appl Math 2017;12:113—20.
24. Aggarwal S, Mishra R, Chaudhary A. A comparative study of Mohand and Elzaki transforms. Glob J Eng Sci Res 2019;6:203—13.
25. Shah R, Khan H, Farooq U, Baleanu D, Kumam P, Arif M. A new analytical technique to solve a system of fractional-order partial differential equations. IEEE Access 2019;7:150037—50.
26. Al-Sawalha MM, Shah R, Khan A, Ababneh OY, Botmart T. Fractional view analysis of Kersten-Krasil'shchik coupled KdV-mKdV systems with non-singular kernel derivatives. AIMS Math 2022;7:18334—59.
27. Khan H, Shah R, Kumam P, Baleanu D, Arif M. An efficient analytical technique, for the solution of fractional-order telegraph equations. Mathematics 2019;7:426.
28. Khan NA, Khan H, Ali SA. Exact solutions for MHD flow of couple stress fluid with heat transfer. J Egypt Math Soc 2016;24:125—9.
29. Islam S, Zhou CY. Exact solutions for two dimensional flows of couple stress fluids. Z Angew Math Phys 2007;58:1035—48.
30. Gaikwad SN, Kouser S. Double diffusive convection in a couple stress fluid saturated porous layer with an internal heat source. Int J Heat Mass Tran 2014;78:1254—64.
31. Shah R, Farooq U, Khan H, Baleanu D, Kumam P, Arif M. Fractional view analysis of third-order Kortewege-De Vries equations, using a new analytical technique. Front Phys 2011;7:244.
32. Khader MM, Adel M, Messaoudi M. Modeling and numerical simulation of Maxwell nanofluid ow with heat generation and convective heating: a combined Adomian decomposition method and Mohand transform. Bound Value Probl 2025;66:1—16.
33. Parand K, Delkhosh M. Operational matrices to solve nonlinear Volterra-Fredholm integro-differential equations of multi-arbitrary order. Gazi Univ J Sci 2016;29:895—907.
34. Abdelrazec A, Pelinovsky D. Convergence of the Adomian decomposition method for initial-value problems. Numer Methods Part Differ Equ 2011;27:749—66.

35. Cherruault Y. Convergence of Adomian's method. Math Comput Model 1990;14:83—6.
36. El-Kalla IL. Convergence of the Adomian method applied to a class of nonlinear integral equations. Appl Math Lett 2008;21: 372—6.
37. Hassan K, Farooq U, Rasool S, Arif M. Analytical solutions of (2+time fractional order) dimensional physical models, using modified decomposition method. Appl Sci 2020;10: 1—20.
38. Masood S, Hajira KH, Shah R, Mustafa S, Khan Q, Arif M, et al. A new modified technique of Adomian decomposition method for fractional diffusion equations with initial boundary conditions. J Funct Spaces 2022;6890517:1—12.
39. Turkyilmazoglu M. The analytical solution of mixed convection heat transfer and fluid flow of an MHD viscoelastic fluid over a permeable stretching surface. Int J Mech Sci 2013;77:263—8.
40. Yih KA. Free convection effect on MHD coupled heat and mass transfer of a moving permeable vertical surface. Int Commun Heat Mass Tran 1999;26:95—104.
41. Marliadi S, Nadihah W, Adem K. A fractional model of Abalone growth using Adomian decomposition method. Eur J Pure Appl Math 2025;18:5799.
42. Javed I, Iqbal S, Ali J, Siddique I, Younas MH. Unveiling the intricacies: analytical insights into time and space fractional order inviscid Burger's equations using the Adomian decomposition method. Partial Differ Equ Appl Math 2024;11:100817.